# Blind Separation of Signal and Multipath Interference for Synthetic Aperture Sonar

Ivars P. Kirsteins
Naval Undersea Warfare Center, Code 8212, Newport, RI 02841-1708 USA
e-mail: kirsteinsip@npt.nuwc.navy.mil

***Abstract*- Multipath interference is a major source of noise for synthetic aperture sonar systems operating in shallow water. Motivated by this problem, we present an iterative algorithm for blindly separating the signal from the multipath interference that uses differences in the temporal coherence properties of the signal and multipaths caused by sea surface roughness to estimate the optimum filter weights. The filter weights are estimated by minimizing the circular variance of the phase differences between overlapping vertical phase centers. An important advantage of this approach is that signal-free training data and accurate array calibration information are not needed. Experimentally we show that the blind separation performance is competitive with high resolution angle of arrival estimation and compares favorably to the Cramer-Rao lower bound predicted error.**

## I. INTRODUCTION

Synthetic aperture sonar (SAS) is commonly used in applications requiring high resolution seafloor images such as bottom mapping, mine hunting, cable and pipeline surveying, and underwater archaeology. Fine cross-range resolution is obtained using the motion of the sonar platform to synthesize a much larger virtual acoustic aperture or baseline than the sonar's physical aperture by coherently combining echoes from multiple pings [1]. In addition to volume and surface reverberation, an important source of interference for SAS in shallow water is corruption by bottom reverberation components propagating into the receiver via surface-bounce multipaths (see fig. 1). Multipath interference is detrimental to SAS image quality. Fig. 2 shows an artificial SAS image with and without multipath interference in shallow water from a patch of reverberation containing a target casting a shadow on the seafloor. The multipath interference adds noise to the SAS image and obscures target structures such as shadows. Another effect is the inability to coherently focus the multipath components because they have been decorrelated by sea surface roughness, resulting in blurring [2]. Multipath interference becomes particularly severe when the range $R$ is much greater than the water depth $L$, that is, $R >> L$.

In principle, a vertical array receiver could be used to null or attenuate the multipath interference by forming delay-sum beams steered toward the bottom to suppress interference components coming from surface directions. However, the closeness of the multipath angles at longer ranges and the presence of higher-order multipaths, i.e., paths involving a surface and bottom bounce, necessitates the use of unrealistically large vertical arrays (space constraints of the SAS vehicle limit the size of the vertical aperture) to obtain the angular resolution needed for sufficient multipath attenuation.

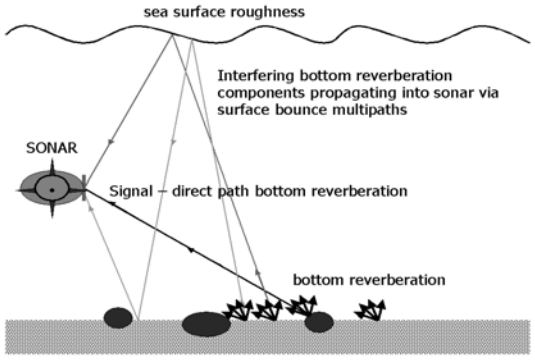


Fig. 1. Depiction of bottom reverberation components propagating to the sonar receiver over surface bounce multipaths.

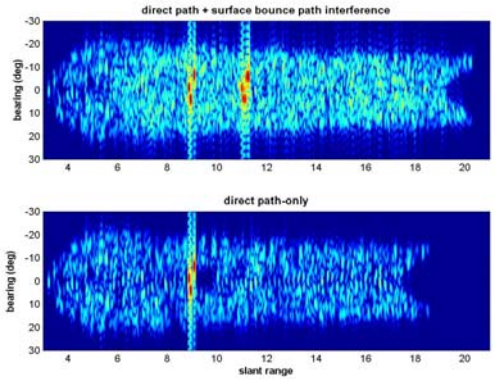


Fig. 2. Artificial SAS image with and without multipath interference containing a target that casts a shadow on the bottom. The multipath interference fills in the target shadow.

Alternatively, a small vertical array could be combined with an adaptive method such as a generalized sidelobe canceller (GSC) [3] to null the multipath interference. However, application of adaptive interference cancellers here is complicated by the simultaneous presence of both signal and multipath interference (i.e. signal contaminated training data) which results in slow convergence and signal cancellation (see Boroson [4]). GSCs are also prone to signal cancellation from errors in the signal blocking matrix caused by array calibration and signal beam pointing errors.

# Report Documentation Page

*Form Approved*
*OMB No. 0704-0188*



| 1. REPORT DATE | 2. REPORT TYPE | 3. DATES COVERED |
|---|---|---|
| **01 SEP 2003** | **N/A** | **-** |

| 4. TITLE AND SUBTITLE | 5a. CONTRACT NUMBER |
|---|---|
| **Blind Separation of Signal and Multipath Interference for Synthetic Aperture Sonar** | 5b. GRANT NUMBER |
| | 5c. PROGRAM ELEMENT NUMBER |
| 6. AUTHOR(S) | 5d. PROJECT NUMBER |
| | 5e. TASK NUMBER |
| | 5f. WORK UNIT NUMBER |
| 7. PERFORMING ORGANIZATION NAME(S) AND ADDRESS(ES) **Naval Undersea Warfare Center, Code 8212, Newport, RI 02841-1708 USA** | 8. PERFORMING ORGANIZATION REPORT NUMBER |
| 9. SPONSORING/MONITORING AGENCY NAME(S) AND ADDRESS(ES) | 10. SPONSOR/MONITOR'S ACRONYM(S) |
| | 11. SPONSOR/MONITOR'S REPORT NUMBER(S) |

12. DISTRIBUTION/AVAILABILITY STATEMENT
**Approved for public release, distribution unlimited**

13. SUPPLEMENTARY NOTES
**See also ADM002146. Oceans 2003 MTS/IEEE Conference, held in San Diego, California on September 22-26, 2003. U.S. Government or Federal Purpose Rights License., The original document contains color images.**

14. ABSTRACT

15. SUBJECT TERMS

| 16. SECURITY CLASSIFICATION OF: | | | 17. LIMITATION OF ABSTRACT | 18. NUMBER OF PAGES | 19a. NAME OF RESPONSIBLE PERSON |
|---|---|---|---|---|---|
| a. REPORT | b. ABSTRACT | c. THIS PAGE | | | |
| **unclassified** | **unclassified** | **unclassified** | **UU** | **8** | |

Motivated by these problems, we had proposed in [5] a method for blindly separating the signal from multipath interference that estimated the separation filter weights by maximizing the ping-to-ping phase coherence, exploiting the decorrelated nature of the multipath interference, rather than a least-squares criterion vis-à-vis a GSC. It works well while not needing precise array calibration information or signal-free training data. However, the preliminary formulation in [5] required multiple pings from fixed sonar positions for adaptation, which may be difficult to acquire in an actual SAS system because of platform motion. In this paper we extend the separation methodology to a moving SAS system. An outline of the paper is presented below:

2) **Problem formulation:** The mathematical representations of the received signal plus multipath interference are developed and we describe how pairs of vertical array measurements with correlated bottom signals can be obtained by adjusting the forward motion of the SAS vehicle so that the array phase centers overlap between any two successive pings.
3) **Optimum filtering and canonical correlation-based blind separation:** We review optimum filtering and show that the optimum filter weights can also be determined blindly (without needing a signal replica) by designing filter weights to maximize the output correlation between overlapping array phase centers, taking advantage of the correlated nature of the bottom signal between any two successive pings.
4) **Blind estimation of filter weights:** Instead of using canonical correlation analysis, we advocate estimating the filter weights by minimizing the circular variance of the phase differences between overlapping array phase centers and motivate why the circular variance is a good measure of phase coherence.
5) **Numerical Results:** Numerical results are presented comparing the new method against the CRLBs, a high resolution angle of arrival estimation algorithm, conventional beamforming, and ideal null-steering, showing that the blind method works well and does not incur much performance loss relative to parametric methods.

## II. PROBLEM FORMULATION

Suppose the SAS system has a planar array as a receiver and a point source transmitter. For the sake of simplicity, (without loss in generality) assume that it consists of only two columns of equi-spaced hydrophones and a transmitter located at the center (see fig. 3). Denote the complex vertical aperture sensor or beam outputs (at a given frequency) containing the backscattered bottom signal and multipath components impinging on the leftmost and rightmost staves from a given range cell in the kth ping cycle as $\vec{x}_k$ and $\vec{y}_k$ respectively. We can then model the stave outputs as

$$\vec{x}_k = \underbrace{\alpha_k^x \vec{s}}_{\text{signal}} + \underbrace{\sum_{j=1}^{P} c_{jk}^x \vec{h}_j}_{\text{multipaths}} + \vec{n}_k^x , \tag{2.1}$$

and

$$\vec{y}_k = \underbrace{\alpha_k^y \vec{s}}_{\text{signal}} + \underbrace{\sum_{j=1}^{P} c_{jk}^y \vec{h}_j}_{\text{multipaths}} + \vec{n}_k^y , \tag{2.2}$$

where the vector $\vec{s}$ is the signal basis vector or array manifold, $\vec{h}_j$ is the basis vector of the jth multipath interference component, P is the number of interfering multipaths, $\alpha_k^x, \alpha_k^y$ are the complex signal amplitudes, the $c_{jk}$ are complex random variables corresponding to the interference amplitudes, and the elements of the background noise vector $\vec{n}_k^x, \vec{n}_k^y$ correspond to volume and surface reverberation and ambient noise.

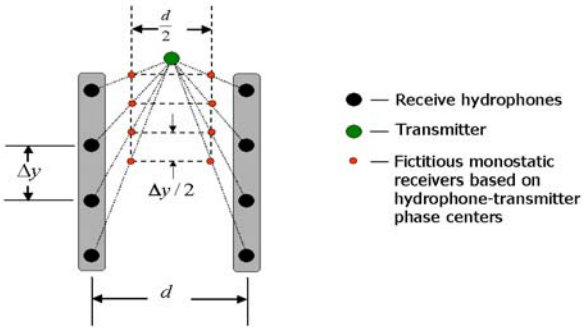


Fig. 3. Planar array geometry and creation of fictitious monstatic elements using the phase centers of the receiver-transmitter pairs.

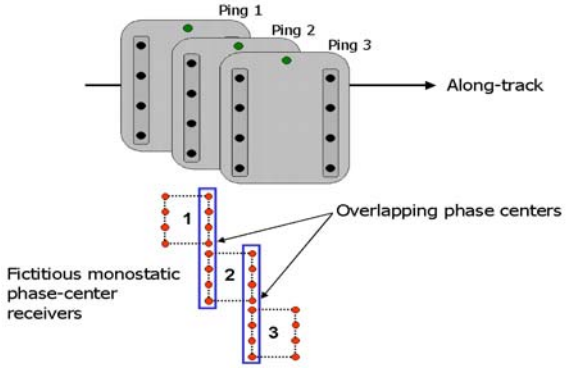


Fig. 4. Overlapping vertical phase centers obtained by adjusting the ping repetition rate and the SAS vehicles forward speed.

Although each receiver-transmitter pair has a bistatic geometry, they can be approximated by an equivalent fictitious monostatic receiver-transmitter located at their mid-point (see fig. 3) [6,7]. This approximation holds as long $\Delta^2 / 4r << \lambda$ where $\Delta$ is the distance between the receiver and transmitter, r is the range, and $\lambda$ is the signal wavelength [7]. That is, the backscattered signal measured from the seafloor by the bistatic receiver-transmitter pair is approximately the same as that would be measured by a single receiver-transmitter located at their phase center. If we adjust the speed of the SAS vehicle and the ping repetition rate such that the array is displaced by distance d/2 between successive pings, the array phase centers will overlap, as depicted in fig. 4. Therefore the stave receiver-transmitter pairs corresponding to the overlapping fictitious monostatic elements will measure the same bottom signal. This is the principle that is used by the method of displaced phase centers for SAS motion compensation [6,7].

Thus for any pair of overlapping fictitious staves, we have $\alpha_k^x \approx \alpha_{k+1}^y$. Because of sea surface roughness, we will also assume that the multipaths are uncorrelated from ping-to-ping and path-wise. A reasonable model for the signal and multipath interference amplitudes and the background noise is that they are zero-mean complex Gaussian distributed [3] with covariance matrices

$$R_x = R_y \equiv \lambda_s \vec{s}\vec{s}^{\,H} + \underbrace{\sum_{j=1}^{P} \lambda_j \vec{h}_j \vec{h}_j^{\,H} + \sigma^2 I}_{R_I} \qquad (2.3)$$

and

$$R_{xy} = E[\vec{x}_k \vec{y}_{k+1}^{\,H}] = \rho \lambda_s \vec{s}\vec{s}^{\,H} \quad , \qquad (2.4)$$

where $\lambda_j$ is the power of the jth path and $\rho$ is the correlation coefficient between $\alpha_k^x$ and $\alpha_{k+1}^y$.

## III. OPTIMUM FILTERING AND CANONICAL CORRELATION-BASED BLIND SEPARATION

Our objective is to estimate the signal expansion coefficients $\alpha_k^x$ in the $\vec{x}_k$ (2.1) in the presence of multipath interference. The minimum least-squares error estimate of the signal expansion coefficient $\alpha_k^x$ is given by $\hat{\alpha}_k = \vec{w}_o^{\,H} \vec{x}_k$ where $\vec{w}_o = R_I^{-1}\vec{s} / (\vec{s}^{\,H} R_I^{-1} \vec{s})$ [8]. These filter weights also maximize the output signal-to-noise ratio [8]. This of course assumes that we know the interference covariance matrix $R_I$ and the signal replica $\vec{s}$. Suppose for a moment that $\vec{s}$ is not accurately known because of array calibration errors and uncertainty in the signal arrival direction. Is there a way to determine the optimum filter weights without needing $\vec{s}$, that is, blindly find $\vec{w}_o$. Recall that in our problem, pairs of signal and noise measurements $(\vec{x}_k, \vec{y}_{k+1})$ from overlapping phase centers are observed in which the signal is highly correlated between the vector pairs, but the interference is uncorrelated. It turns out that these differences in correlation properties between signal and interference can be used to blindly determine the optimum filter weights without needing knowledge of the signal replica [9]. Using the results of [9] here, the filter weights that maximize the output correlation $E[\vec{w}^H \vec{x}_k \vec{y}_{k+1}^{\,H} \vec{w}]$ between two overlapping phase centers subject to the constraint that $Var[\vec{w}^H \vec{x}_k] = 1$ are *proportional* to the *optimum filter weights* $\vec{w} = R_I^{-1}\vec{s}$ and can be calculated from $R_x$ or $R_y$ and $R_{xy}$ by solving the eigen-equation

$$R_{xx}^{-1} R_{xy} R_{xx}^{-1} R_{xy}^{H} \vec{w} = \lambda \vec{w} \qquad (3.1)$$

for $\lambda$ and $\vec{w}$. This method of calculating the filter weights is based on the technique of canonical correlation analysis from multivariate statistics. The statistician Hotelling developed canonical correlation analysis in the 1930s for exploring dependencies or relationships between random vectors [10] and today is a standard statistical analysis tool. The approach is useful because it is does not need signal-free interference measurements (i.e. works with signal contaminated data) or a precise signal replica.

However, in our case both $R_x$ and $R_{xy}$ are unknown. It is easy to convince oneself that plugging estimates of $R_x$ and $R_{xy}$ into (3.1) and solving for $\vec{w}$ does not generally maximize the true output cross-correlation

$$\hat{c}(\vec{w}) = \frac{\sum_k \vec{w}^H \vec{x}_k \vec{y}_{k+1}^{\,H} \vec{w}}{(\sum_m |\, \vec{w}^H \vec{x}_m \,|^2)^{1/2} (\sum_n |\, \vec{w}^H \vec{y}_{n+1} \,|^2)^{1/2}} \quad . \qquad (3.2)$$

This suggests that an estimate based on (3.1) is likely to be poor. An additional concern is that canonical correlations needs high stability in both magnitude and phase of the transmitted and received signal. Magnitude stability in practice is more difficult to achieve than phase stability because of transmitter electronics fluctuations. Thus we advocate designing the filter weights by directly maximizing the phase coherence between the $(\vec{x}_k, \vec{y}_{k+1})$ pairs rather than indirectly using estimated covariances. In the next section we present an iterative approach for estimating the optimum filter weights that is based on minimizing the circular variance of the phase differences only.

## IV. BLIND ESTIMATION OF FILTER WEIGHTS

We want to estimate the optimum filter weights from K independent pairs of signal and interference measurements $(\vec{x}_1, \vec{y}_2), \ldots, (\vec{x}_K, \vec{y}_{K+1})$ by maximizing the output phase

coherence measured between the pairs using some metric. One way of quantitatively measuring the phase coherence between $\vec{w}^H \vec{x}_k$ and $\vec{w}^H \vec{y}_{k+1}$ is to calculate the phase difference $\angle \vec{w}^H \vec{x}_k - \angle \vec{w}^H \vec{y}_{k+1}$ where the operator $\angle \cdot$ means the argument of the complex number, i.e., angle or phase. Following this idea, a reasonable approach then might be to estimate the filter weights by minimizing the mean-square phase difference between the overlapping phase centers, i.e., solving

$$\min_{\vec{w}} \quad \sum_k \left( \angle \vec{w}^H \vec{x}_k - \angle \vec{w}^H \vec{y}_{k+1} \right)^2 \quad . \tag{4.1}$$

However, numerical evaluation of phases is hard because their cyclical nature (modulo $2\pi$) may require phase unwrapping. This difficulty can be overcome by using the *circular variance* [11,12]. The *circular variance* (CV) is defined for given a set of angle measurements $\phi_1,\ldots,\phi_N$ as

$$\begin{aligned} cv[\phi] &= 1 - \sqrt{\bar{x}^2 + \bar{y}^2} \\ \bar{x} &= \frac{1}{N} \sum_{n=1}^{N} \cos(\phi_k) \\ \bar{y} &= \frac{1}{N} \sum_{n=1}^{N} \sin(\phi_k) \end{aligned} \tag{4.2}$$

and lies in the interval [0, 1], with one corresponding to maximum variance. It is easy to evaluate numerically and commonly used in analyzing the dispersion of angular data such as wind and ocean current direction, fracture orientations, and animal movements. The CV is also related to the maximum likelihood (ML) estimate of the concentration parameter of the von Mises distribution [11]

$$p_{VM}(\phi) = [2\pi I_0(k)]^{-1} e^{\kappa \cos(\phi - \bar{\phi})} \ , \ 0 \le \phi \le 2\pi \quad , \tag{4.3}$$

through the relation $1\text{-}CV = I_1(\kappa)/I_0(\kappa)$ where $\kappa$ is the concentration parameter, $\bar{\phi}$ is the mean angle, and $I_m(k)$ is the modified Bessel function of order m. The von Mises distribution is often used to model circular or angular data and is considered to be the circular analog of the regular Gaussian distribution [11,12] and approaches the Gaussian distribution as $\kappa \to \infty$ [11]. This suggests that the CV is likely a good measure of phase dispersion or coherence. Viterbi also showed that (4.3) is the probability density for the carrier phase estimate of a sinusoidal signal in noise obtained by first-order phase-locked loop and that the concentration parameter $\kappa$ is proportional to signal-to-noise ratio [13]. The CV has also been previously used in frequency estimation and can be interpreted as a type of circular regression in that problem at high signal-to-noise ratios [14].

Based on the above discussions, we propose estimating $\vec{w}$ by minimizing the circular variance of the output phase differences,

$$cv[\vec{w}] = 1 - \left| \frac{1}{K} \sum_{k=1}^{K} e^{i(\angle \vec{w}^H \vec{x}_k - \angle \vec{w}^H \vec{y}_{k+1})} \right| \quad . \tag{4.4}$$

with $\vec{w}$ constrained to be non-zero to avoid getting a trivial solution. Fig. 5 shows a comparison of the proposed blind method to the conventional GSC.

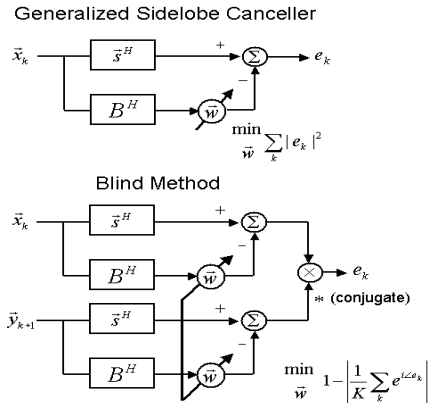


Fig. 5. Comparison of the blind method against the conventional GSC where B is the signal-blocking matrix.

Since no closed form solution is available for the above minimization problem, some form of iterative search is required, e.g. steepest descent, quasi-Newton etc [15]. We chose to use the Fletcher-Reeves (FR) method [15] for performing the optimization. The search direction for the kth FR iteratation is given by

$$\vec{d}_k = -\vec{g}_k + (\|g_k\|_F^2 / \|g_{k-1}\|_F^2) \vec{d}_{k-1} \quad , \tag{4.5}$$

where $\vec{g}_j$ is the gradient of the phase variance $cv[\vec{w}]$ evaluated using the iterate from the jth step. The updated weight vector estimate $\vec{w}_k = \vec{w}_{k-1} + \lambda \vec{d}_k$ is found by minimizing $cv[\vec{w}_{k-1} + \lambda \vec{d}_k]$ with respect to $\lambda$. This method is simple and has quadratic-like convergence [15]. We will discuss starting points and convergence in more detail later.

This procedure is "blind" because the signal replica $\vec{s}$ is not needed for estimating the weight vector. But $\vec{w}$ can be only be uniquely determined up to a scale factor. If the time series is to be reconstructed after doing the separation in the frequency domain, then at least some partial knowledge of the array geometry and calibration is needed to maintain unit gain signal response for the signal reconstruction.

*A. Optimality of the Circular Variance*

For a given set of filter weights, formula (4.4) is a function of the phase differences between two correlated complex Gaussian random variables, i.e., $\phi = \angle \vec{w}^H \vec{x}_k - \angle \vec{w}^H \vec{y}_{k+1}$. Their probability density is given by (see [16] and also [17])

$$p_{CG}(\phi | \vec{w}) = \frac{(1-\rho^2)[(1-\beta^2)^{1/2} + \beta(\pi - \cos^{-1}\beta)]}{2\pi(1-\beta^2)^{3/2}} \quad , (4.6)$$

where $\beta = \rho\cos(\phi - \bar{\phi})$ and ρ is the correlation between $\vec{w}^H \vec{x}_k$ and $\vec{w}^H \vec{y}_{k+1}$. By inspection (4.6) is not the same as the von Mises density (4.3). Since we are implicitly seeking to maximize the correlation between the filter outputs by minimizing the phase circular variance, a question arises as to how well the CV characterizes the correlation between complex Gaussian random variates. Since density (4.6) is a function of the correlation coefficient ρ, it would be desirable prove sufficiency [18] or at least approximate sufficiency of the CV for ρ. However, this appears difficult. In appendix A, we looked at the related hypotheses testing problem of determining whether a given population is distributed as ρ=0 (uniform) or ρ>0 using 1-CV and the likelihood ratio (LR) as test statistics and show numerically that the CV appears to "capture" much of the information regarding ρ.

## V. NUMERICAL RESULTS

Here we present some numerical results investigating the error surface and comparing the blind separation method by computer simulation against high resolution angle estimation, Cramer-Rao lower bounds [18], conventional beamforming and the clairvoyant null-steerer and an artificial SAS image example. We begin by discussing the experimental scenario.

The SAS system is modeled as having a 10 element equi-spaced vertical array receiver and ensonifies the bottom with a monochromatic signal pulse in each ping cycle. One signal is directly backscattered from the bottom to the receiver and another arrives to the receiver via a surface bounce path, with both arrivals modeled as plane waves (see fig. 1). Two overlapping phase center pairs $(\vec{x}_k, \vec{y}_{k+1})$ are collected in each SAS cycle and are modeled as being jointly complex Gaussian distributed with the covariance and cross-covariance matrices of (2.3) and (2.4) respectively. Their parameters were set to $\lambda_S$=1, ρ=.95 (ping-to-ping signal correlation), $\lambda_1$=1 (the signal and multipath interference have the same power), and $\sigma^2$=.01. The new blind method was implemented in beamspace analogous to that of a GSC, i.e., using the outputs of two beams, one steered at the desired bottom signal, and a interference reference beam orthogonal to the signal steered at the multipath interference (like in fig. 5). This is equivalent to operating on the transformed data $\vec{u}_k = B^H \vec{x}_k$ and $\vec{v}_k = B^H \vec{y}_{k+1}$, where B is a $10 \times 2$ matrix whose columns correspond to the bottom and surface steering replica vectors.

*A. Circular Variance Surface*

In the first experiment, we examined the shape of the circular variance surface as a function of the filter weights for insight into the difficulty of using gradient-based iterative search methods. Since only one multipath component is present, the weight vector in formula (4.4) can be written as $\vec{w} = [1\ (a_r + ia_i)]^T$. K=10, 20, 30, and 40 independent data snapshots pairs were computer generated using (2.1) and (2.2) and plugged into the circular variance formula (4.4) and plotted in fig. 6 as a function of $a_R$ and $a_I$. We see that as the number of data

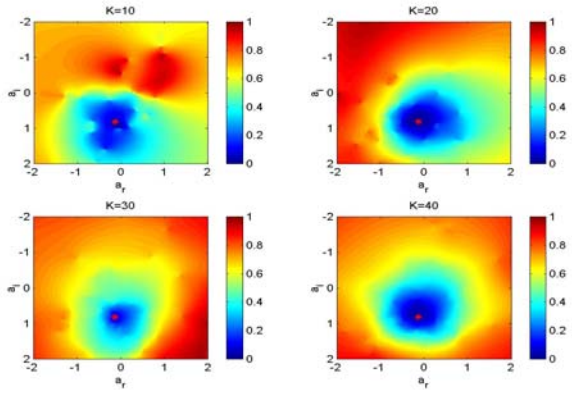


Fig. 6. The output circular variance plotted as a function of $a_R$ and $a_I$ for K=10, 20, 30 and 40 independent data snapshot pairs. The symbol "*" corresponds to the optimum filter weight values.

snapshots increases, the surface tends to become more regular or quadratic-like with the circular variance minima being close to that of the optimum filter weights. However, surface irregularities and local stationary points do occasionally occur outside the concave region surrounding the global minima as seen in fig. 6, suggesting that it is important to have a good starting weight vector to avoid getting stuck in local stationary points during the iterative search. Some possible approaches for obtaining good starting vectors for the Fleetcher-Reeves method [15] include using the GSC filter weight estimate or its gradient as an initial search direction or using prior information about the geometry (sonar and water depth, and range) or computing the differences $\vec{x}_k - \vec{y}_{k+1}$ to obtain a nearly signal-free data set to estimate an initial guess (it can be argued that if the signal is highly correlated between the phase center pairs, this procedure will remove most of the signal assuming no transmitter magnitude fluctuations).

*B. 1-Multipath Performance Evaluation*

The performance of the blind method is now compared against the Cramer-Rao lower bound (CRLB) (see the CRLB derivation in appendix B), high resolution angle of arrival estimation algorithm of Kumaresan and Tufts [19], the clairvoyant null-steerer (constructed using perfect knowledge of signal and interference arrival directions), and the conventional beamformer. 30 independent data pairs were computer generated in each trial according to the experimental scenario described at the beginning of this section and both the blind method and the minimum-norm methods were implemented (the minimum-norm method estimated the signal by first estimating the signal and interference spatial frequencies and then fitting plane-waves of those frequencies in a least-squares sense to the observed data). The blind method was implemented using an initial guess of $\vec{w}_0 = [1\ 0]^T$ to start the Fletcher-Reeves algorithm. Both the error in estimating the weight vector (nominal weight vector subtracted from estimated weight vector) and the signal ($\hat{\alpha}_1^x = \vec{w}^H \vec{x}_1$) were tabulated. A total of two thousand independent computer simulation trials were performed at different spatial separations to measure the mean-square-errors (MSEs).

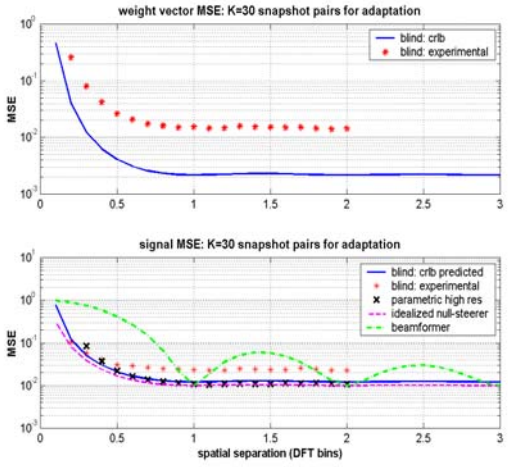


Fig. 7. The measured MSE of the blind method (weight vector and signal estimation errors) plotted as a function of signal and interference separation in DFT bins and compared against the high resolution angle of arrival estimation algorithm, the CRLB, conventional beamformer, and clairvoyant null-steerer.

The lowermost plot of fig. 7 compares the signal estimation MSE of the blind method against the high resolution method, the CRLB (see appendix), clairvoyant null-steerer, and conventional beamformer as a function of signal and interference vertical separation in DFT bins. We see that the blind method performs well with respect to the other methods, and becomes very competitive against the parametric high resolution method once the signal and interference are within a ½ DFT bin width of each other. We also see that the blind method signal MSE is fairly close to that predicted by the CRLB (see appendix B). The uppermost plot of Fig. 7 compares the weight vector estimation error against the CRLB for the weight vector (see appendix B). Although the blind method does not approach the CRLB, we must bear in mind that the CRLBs were derived assuming that both signal magnitude and phase information are used in the estimation process, whereas the blind method uses only phase information. Next, the experiment was repeated with the spatial separation set to ½ DFT bin and the number of data snapshots pairs used for estimating the weight vector varied from 10 to 100 (see fig. 8). As expected, the uppermost plot of Fig. 8 shows that blind method does not approach the weight vector CRLB as the number of snaphot pairs K increases. However, in terms of the signal estimation MSE, the blind approach performs well and is close to that of the high resolution angle estimation method.

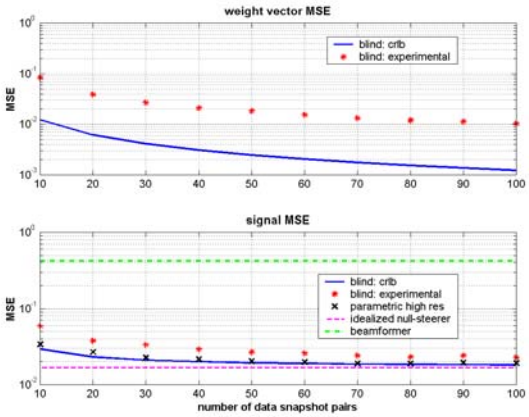


Fig. 8. The measured MSE of the blind method (weight vector and signal estimation errors) plotted as a function of the number of data snapshot pairs for used adaptation and compared against the CRLBs and the other methods.

*C. 2-Multipath Artificial SAS Image Example*

In the last example, we simulate a two multipath interference situation (a surface and surface-bottom path) and show that the blind method outperforms the generalized sidelobe canceller and the conventional beamformer in terms of SAS image quality. The same experimental scenario is used as before, except for the presence of a surface-bottom path and an object casting a shadow on the seafloor. The direct path bottom signal was separated vertically from the surface path in spatial frequency by .4 DFT bins and by -.7 DFT bins from the surface-bottom path. The surface and surface-bottom path reverberation levels were set to the same power and a total of 40 data snapshot pairs were collected for processing while the SAS system

moved on a linear track. The GSC was implemented erroneously (signal reference and signal-blocking interference reference beams constructed using incorrect signal direction information) with the assumed signal direction mismatched by .2 DFT bins away from the actual signal direction.

Fig. 9 shows the SAS images generated using the conventional beamformer (a beam steered toward the bottom), the blind separation method, and the GSC. Note that the object shadow occurs in range cells 30-40. By visual inspection, we see that the object shadow in the conventional beamformer image is barely perceptible, i.e., obscured by the multipath interference. The GSC image shadow quality is somewhat better, although the shadow area still contains considerable multipath leakage. The SAS image obtained from the blind method has the best shadow quality out of the three methods. The GSC performed poorly because of signal contamination in both the signal reference beam and the signal-blocking interference reference beams.

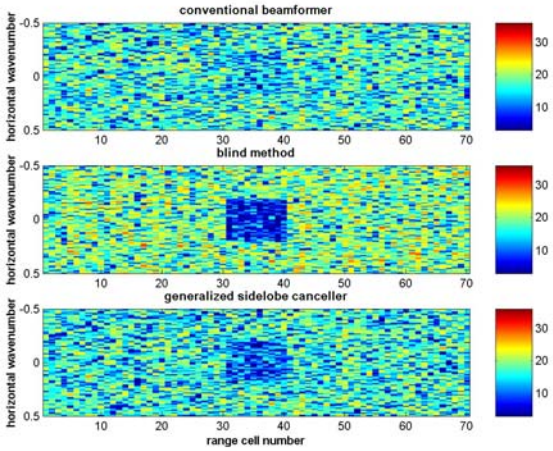


Fig. 9. Artificial SAS images created after multipath rejection using conventional beamforming (top), blind separation (middle), and GSC (bottom). Note that all of the methods were applied in the vertical domain and the true object shadow occurs between range cells 30-40.

## VI. CONCLUDING REMARKS

These results suggest that blind separation of the signal from the multipath interference is competitive with high resolution angle of arrival estimation algorithms and compares favorably to the CRLB-predicted signal MSE. An important advantage of doing the separation blindly is that signal-free training data and highly accurate array calibration information are not needed, unlike high resolution methods or GSCs. However, more work is needed in understanding the convergence properties of the iterative scheme and performance as the number of multipaths increases.

## APPENDIX A: OPTIMALITY OF THE CV

One approach for getting insight into the sufficiency of the CV for $\rho$ is to look at the hypotheses testing problem of determining whether K independent phase difference measurements are distributed according to $\rho$=0 (uniform) or $\rho$>0 using 1-CV and the likelihood ratio (LR) (constructed using density (4.6) and assuming the mean phase is unknown) as test statistics. We implemented and evaluated the performance of the two detectors for 5, 10, 20, and 30 independent and identically distributed phase measurements (number of measurements is denoted as K in the paper) using 5000 independent computer simulation trials and tabulated the probability of detection as a function of correlation $\rho$ with the probability of false alarm set to $10^{-2}$. The results in fig. 10 show that the CV performs nearly as well as the optimum LR detector, suggesting that the CV is a good measure of correlation for this problem and is likely nearly sufficient at least in these examples.

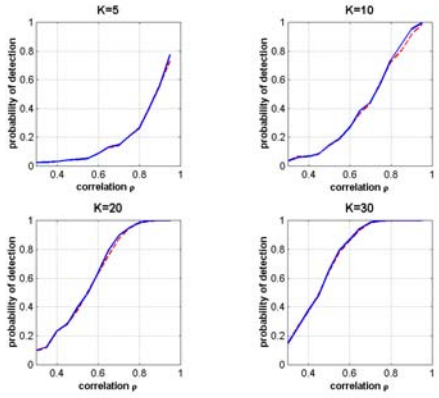


Fig. 10. The measured probability of detection vs. $\rho$. The blue and red dashed lines correspond to the likelihood ratio and circular variance test statistics respectively.

## APPENDIX B: CRAMER-RAO LOWER BOUNDS

Here we describe the steps for deriving the Cramer-Rao lower bounds on the error in estimating the filter weights and bounding the signal estimation error from K independent pairs of signal and interference measurements $(\vec{x}_1, \vec{y}_2), \ldots, (\vec{x}_K, \vec{y}_{K+1})$ for the two channel case. We assume that nothing is known about the signal and interference. Suppose for a moment that there is no additive white noise ($\sigma^2$=0) and the signal is perfectly correlated between the pairs $(\vec{x}_k, \vec{y}_{k+1})$. Then the filter weights which provide the best phase coherence (or set the CV to zero) must be the null-steerer

$$\vec{w}_{opt} \propto \vec{h}_{\perp} = (I - \vec{h}\vec{h}^{H})\vec{s} \quad . \qquad \text{(B.1)}$$

The optimum filter weights $\vec{w}_o = R_I^{-1}\vec{s}$ also approach (B.1) as the multipath interference becomes much stronger than the background noise, i.e., $\lambda_1 >> \sigma^2$ [20]. From (B.1), another interpretation of the weight vector estimation problem is one of estimating the part of the signal $\vec{h}_{\perp}$ that lies in the orthogonal complement of the space spanned by the interference basis vectors.

In the two channel case, if $\vec{h} = [-\bar{a}\ 1]^T$, then we have $\vec{h}_{\perp} = [1\ a]^T$. Using the above interference-based coordinate system, the signal basis vector can now be expanded as

$$\vec{s} = (\vec{h}_{\perp} + \beta\vec{h}) / \left\| \vec{h}_{\perp} + \beta\vec{h} \right\|_F \quad . \qquad \text{(B.2)}$$

Recall that the joint complex Gaussian distribution of the data pairs $(\vec{x}_k, \vec{y}_{k+1})$ is characterized by the covariance matrices of (2.3) and (2.4). Plugging (B.2) into (2.3) and (2.4) ($\sigma^2$ cannot be estimated uniquely here because we only have two channels or degrees of freedom), the unknown parameters to be estimated are *a*, $\beta$, $\lambda_S$, $\lambda$, and $\rho$. The elements of the Fisher information are easy to evaluate for this problem and are given by [18]

$$\lfloor J \rfloor_{mn} = tr[R^{-1}\frac{\partial R}{\partial \theta_m}R^{-1}\frac{\partial R}{\partial \theta_n}] \qquad \text{(B.3)}$$

where $R = \mathrm{cov}([\vec{x}_k^T \mid \vec{y}_{k+1}^T]^T)$ is the nominal data covariance matrix and the notation $\theta_m$ means mth parameter. The bound on the mean square-error in estimating the mth parameter then is

$$E[(\hat{\theta}_m - \theta)^2] \geq \lfloor J^{-1} \rfloor_{mm} \qquad \text{(B.4)}$$

It is straightforward to evaluate (B.3) and (B.4) numerically to obtain the bound on the error in estimating the weight vector $\vec{w}$ or its parameter a.

We can also use the weight vector CRLB to glean insight into the signal estimation error. If the interference covariance matrix is $R_I$ and the bound in estimating a is $\sigma_A^2$, then approximately

$$E[|\hat{\vec{w}}^H x_k - \alpha_k|^2] \approx (1+|a_0|^2)\sigma^2 + \sigma_A^2 \lfloor B^H R_I B \rfloor_{22} \qquad \text{(B.5)}$$

where $a_0$ is nominal value.

## References


[1] M.P. Hayes and P.T. Gough, "Broad-band synthetic aperture sonar," IEEE Journal of Oceanic Engineering, vol. 17, no. 1 pp. 80-94, Jan. 1992.

[2] A. Maguer, S. Fioravanti, and A. Lovik, "Below critical angle detection of buried objects," OCEANS '97, MTS/IEEE Conference Proceedings , Volume 1, 1997,pp. 512 –517.

[3] H.L. Van Trees, Optimum array processing, John Wiley & Sons, 2002..

[4] D.M. Boroson, "Sample size considerations for adaptive arrays," vol. AES-16, no. 4, pp. 446-451, July 1980.

[5] I.P. Kirsteins, **"**Blind separation of signal and reverberation by minimizing the circular variance of the phase," Proc. of Asilomar 2002 Conference, vol. 2, Nov. 2002, pp. 1664-1668.

[6] R.W. Sheriff, "Synthetic aperture beamforming with automatic phase compensation for high frequency sonars," Proc. of Autonomous Underwater Vehicle Technology Symposium, 2-3 Jun 1992, pp. 236 –245.

[7] A. Bellettini and M.A. Pinto, "Theoretical accuracy of synthetic aperture sonar micronavigation using a displaced phase center antenna," IEEE Journal of Oceanic Eng., vol. 27, no. 4, Oct. 2002, pp.780-789.

[8] L.W. Brooks and I.S. Reed, "Equivalence of the likelihood ratio processor, the maximum signal-to-noise ratio filter, and the Wiener filter," IEEE Trans. Aerospace and Electronics Systems, Sept. 1972, pp. 690-692.

[9] J. Galy, C. Adnet, and E. Chaumette, "Blind methods for interference cancellation in array processing," 1997 IEEE DSP Workshop, 1997, pp. 1043-1046.

[10] H. Hotelling, "Relations between two sets of variates," Biometrika, vol. 28, Dec. 1936, pp. 321-377.

[11] K.V. Mardia, Statistics of Directional Data, Academic Press 1972.

[12] N.I. Fisher, Statistical analysis of circular data, Cambridge University Press, 1993.

[13] A.J. Viterbi, "Phase-locked loop dynamics in the presence of noise by Fokker-Plank techniques," Proc. IEEE, vol. 51, Dec. 1963, pp. 1735-1753.

[14] Lovell, B.C.; Kootsookos, P.J.; Williamson, R.C., **"**The circular nature of discrete-time frequency estimates," in Proc. of ICASSP-91, vol. 5, 1991, pp. 3369-3372.

[15] B.S. Everitt, Introduction to optimization methods and their application in statistics, Chapman and Hall, New York, 1987.

[16] D. Middleton, Introduction to statistical communication theory, New York, McGraw-Hill, 1960.

[17] J.S. Lee, K. Hoppel, S.A. Mango, and A.R. Miller, **"**Intensity and phase statistics of multi-look polarimetric SAR imagery," Proc. of IGARSS '93, vol. 2, Aug. 1993, pp. 813-816.

[18] S.M. Kay, Fundamentals of statistical signal processing: estimation theory, Prentice-Hall, 1993.

[19] R. Kumaresan and D.W. Tufts, "Estimating the angles of arrival of multiple plane waves," IEEE Trans. on Aerospace Electr. Sys., AES-19, Jan. 1983.

[20] I.P. Kirsteins and D.W. Tufts, "Adaptive detection using low rank approximation to a data matrix," IEEE trans. on Aerospace and Electronic Systems, Jan. 1994, pp. 55-67.